Quantum-Chemical and Classical-Dynamics Calculations for Penning Ionization H_2O + He*(2^1S) → H_2O^+ + He + e^-. Comparison with the Metastable He*(2^3S)

Toshimasa Ishida[†]

Applied Science, Faculty of Engineering, Shizuoka University, 836 Ohya, Shizuoka, 422 Japan

Received: August 28, 1997; In Final Form: December 19, 1997

An ab initio and trajectory calculation is performed for the Penning ionization system H_2O + He*(2^3S) → H_2O^+($^2B_2$, $^2A_1$, $^2B_2$) + He + e^-. The Feshbach projection-operator method is employed to calculate the potential-energy surfaces (PES) of the resonance state and the partial widths for individual partial ionization. An attractive well near the oxygen lone pairs and a long-range barrier are found. The well is deeper but smaller than the corresponding well for H_2O−He(2^3S). Quasiclassical trajectory calculations are performed at H_2O rotational temperatures of 300, 150, and 25 K based on the PES and the widths. The trajectories are drawn into an attractive H_2O lone pair region less strongly with decreasing rotation frequency than those for the 2^3S system. It is also found that fewer trajectories ionize at lower energy. These two results are due to the long-range barrier and the smaller well of the resonance PES for the present system.

1. Introduction

Superexcited states have been much more accessible than ever with the development of synchrotron radiation and lasers. The states can lead to autoionization because the states are embedded in the ionization continua. Penning ionization is one of these autoionization processes.[1] In the gas phase, Penning ionization is described by the following process:

$$M + A^* \rightarrow M^+ + A + e^-$$

where M is the target molecule and A* is an excited species. The experiments of Penning ionization electron spectroscopy include a type of transition-region spectroscopy because the ionization can occur at any distance between M and A.[2,3]

Siska has recently reviewed the experimental as well as the theoretical work on Penning ionization.[4] A few theoretical studies of Penning ionization systems with the H_2O target molecule have been carried out. Bentley[5] has calculated the H_2O−Ne*(2^3P) potential, and has explained the preference for the A_1 ionization channel. Haug, Morgner, and Staemmler[6] have obtained the H_2O−He*(2^3S) resonance potential and have interpreted their experimental electron spectra of the system using electron distribution in molecular orbitals relevant to the ionization reaction. However, neither widths nor ionization cross sections were calculated in these studies.

In recent years, we have been studying Penning ionization theoretically.[7−12] Recently, we carried out an ab initio calculation for the potential-energy surface (PES) of the resonance state and ionized states and the energy widths for H_2O + He*(2^3S) → H_2O^+($^2B_2$, $^2A_1$, $^2B_2$) + He + e^- and found a selection rule for ionization based on the symmetry of ionized states. The selection rule indicates that totally symmetric ionized states are easier to produce.[9] Furthermore, on the basis of the PES and the widths, we performed a trajectory calculation for this system and predicted the effect of the H_2O rotational temperature on the ionization cross section.[10]

In this paper, we present quantum-chemical and classical-dynamics calculations for H_2O + He*(2^1S) → H_2O^+($^2B_1$, $^2A_1$, $^2B_2$) + He + e^-. We compare the results with those for the H_2O + He*(2^3S) system.[9,10]

The dependence of the Penning ionization cross section on collisional energy was investigated experimentally for the present system, and decrease of the magnitude of the total ionization cross section with increasing energy was reported.[13] Comparison of the calculational results is also made with this experiment.

2. Calculations

Details of the present calculation have been described in previous papers both for the ab initio calculations[9] and the trajectory calculations.[10] Therefore, we describe the calculational methods briefly.

A. Ab Initio Quantum-Chemical Calculation. We employed the Feshbach projection-operator method in order to calculate the PES of the entrance channel (V^*) for H_2O + He* and the ionized states (V^+) for $(H_2O + He)^+$ as well as the partial energy widths ($\Gamma^{(i)}$).[14,15] The total energy width Γ is the sum of the partial widths. In the optical potential treatment, V^* and Γ correspond to the real and imaginary parts of the complex potential. In the Feshbach projection method, the CI space is divided into two subspaces that describe V^* and V^+ plus an emitted electron. The matrix elements between the two subspaces are associated with $\Gamma^{(i)}$ with further approximations.[9]

The basis set employed was a TZP class set augmented with diffuse 2s2p functions on the He atom to describe the 2s orbital of He. We performed state-averaged MC-SCF (multiconfigurational self-consistent field) calculations for the three ionized states of H_2O + He^+($^2B_1$, $^2A_1$, $^2B_2$). Each ionized state was described by one configuration. The molecular orbitals determined by the MCSCF calculations were used for the bases of the CI (configuration interaction) calculations. The SDCI (single- and double-substitution CI) from the H_2O−He(1s2s) configuration was performed. The description of the resonance state is expected to be reasonable because of the multiconfigurational description, although the orbitals used are optimized for the ionized states. In order to describe the resonance state, the ground-state configuration corresponding to H_2O−He($1s^2$)

[†] E-mail: ishida-t@eng.shizuoka.ac.jp. Fax: +81-54-238-4933.

S1089-5639(97)02814-4 CCC: $15.00
Published on Web 03/07/1998

was deleted from the CI space. Thus, the variational collapse to the ground state was prevented. The configuration corresponding to $H_2O-He(1s2s)$ was easily identified. The dimension of the CI matrices was 5860. Coulomb functions were employed to express ejected electrons, and the partial waves of the functions were expanded by the vacant orbitals. The partial waves up to $l = 7$ were considered. The center of the Coulomb functions was located on the H_2O atom. Overlap integrals used to express expansion coefficients were evaluated by numerical integration. We used the double-exponential function formula by Takahashi and Mori[16] for the radial part and employed the Gauss−Legendre formula[17] and the trapezoidal formula for the angular parts. The H_2O molecule was fixed to the experimental equilibrium geometry ($R_{OH} = 0.957$ Å and $\angle HOH = 104.52°$). The potential energies of the ionized states were shifted uniformly to match the asymptotic energies of the corresponding experimental values for $H_2O^+(^2B_1, {}^2A_1, {}^2B_2)$ because it is difficult to accurately reproduce the ionization energies of H_2O. Thus, the wavenumber of the Coulomb functions and state density of the ionized states were based on experimental values. Calculations were performed for He approaches to H_2O from 11 different directions. The directions corresponded to every 45° for polar and azimuthal angles. The number of points calculated was approximately 100.

The codes for the Feshbach projection-operator computations were added to the quantum-chemistry program HONDO7 by Dupuis et al.[18]

B. Dynamical Calculation. In the classical theory of Penning ionization,[19,20] the resonance potential and the energy widths are essential quantities for describing the dynamics.

The real part of the entrance potential for the H_2O-He interaction was fitted to an analytical function including $1/R$, $1/R^2$, $1/R^4$, $1/R^6$, and exponential functions with respect to internuclear distances R.[10]

Fitting was carried out using the Marquardt method,[22] one of the nonlinear least-squares methods. Initial values of the fitting parameters were selected using random numbers, and thousands of trials for seeking the optimum values were carried out. The standard deviation of the fit was 0.0979 eV. This deviation is not very satisfactory, but a fit including additional terms with other different powers in R did not significantly improve the results. Although further refinement, for example, including a dumping factor for the $1/R$ term, would improve the fit, it is not expected that this would significantly change the qualitative features of the dynamics. The energy widths were fitted to cubic spline functions and spherical harmonics.

In the classical treatment,[19,20] the total ionization probability at time t is

$$P(t) = 1 - \exp[-\int_{-\infty}^{t} dt'\, W(t')] \qquad (1)$$

and the partial ionization probability[21] is

$$P^{(i)}(t) = \int_{-\infty}^{t} dt'\, W(t') \exp[-\int_{-\infty}^{t'} dt''\, W(t'')] \qquad (2)$$

where $W(t) = \Gamma(\mathbf{R})/\hbar$ and $W^{(i)}(t) = \Gamma^{(i)}(\mathbf{R})/\hbar$ are the rates of total and partial ionizations, respectively. In this formulation, it can readily be seen that the total-ionization cross section is equal to the sum of the partial-ionization cross sections.

The fourth-order Adams−Moulton predictor−corrector method was used for the quasiclassical-trajectory integration for the present system.[23] The time step was 1.0×10^{-16} s. The rigid-symmetric-rotor approximation[24] was applied to the target H_2O molecule. The distance r(OH) and the angle $\angle$HOH were set

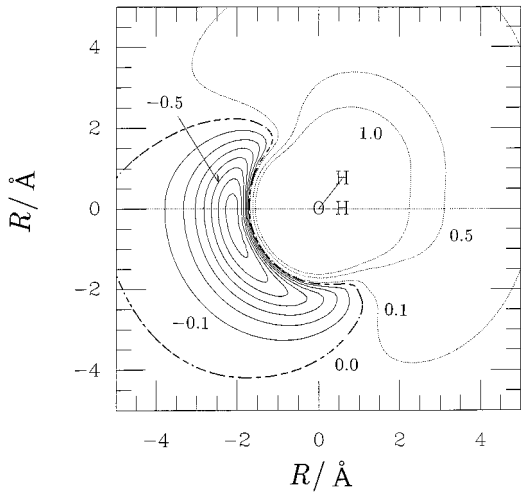

Figure 1. Contour map of the potential-energy surface for the entrance channel $H_2O-He^*(2^1S)$. The upper panel is for the molecular plane, and the lower is for the bisector plane that is perpendicular to the molecular plane. Solid contour lines correspond to −0.1 to −0.7 eV, the dotted lines to 0.1, 0.5, and 1.0 eV from the outside, and the dash−dotted line to 0.0 eV compared to the $H_2O-He^*(2^1S)$ asymptote.

equal to the experimental values above by the imposition of three constraints.[25] The time evolution of the trajectories was ceased when the He atom was separated from the center of gravity of the H_2O molecule by the initial separation of 30 Å. The maximum impact parameter, b_{max}, was taken to be 7 Å.

The initial J and K quantum numbers of a symmetric rotor were selected for each rotational temperature, and the $(J + {}^1/_2)^2$ and K quantities were used to determine an absolute value and the C_2 axis component of the angular-momentum vector, respectively.

Ionization probabilities for total and partial ionization were evaluated for each time step using the fitted energy widths and were integrated to yield probabilities using eqs 1 and 2. Cross sections were obtained from an average of 2000 trajectory calculations for each collisional energy and rotational temperature. In total, 54 000 trajectories were calculated. An importance sampling was employed for the sampling of impact parameters:[25] $b = \xi b_{max}$ was used instead of $b = \xi^{1/2} b_{max}$, where ξ is a random number. This sampling is well-suited to the analysis of the opacity function.

3. Results and Discussion

A. Potential-Energy Surfaces. Figure 1 shows the entrance channel potential V^* for $H_2O + He(2^1S)$. The figure was obtained by interpolation and is the counterpart of Figure 1 of ref 8. The potential V^* has qualitative features similar to that for $H_2O + He(2^3S)$: The potential is attractive near the lone pairs of the H_2O molecule and is strongly repulsive on the side of the hydrogen atoms. The well depth for the present system is about 0.75 eV. This well depth is deeper than the well depth of $H_2O + He(2^3S)$, which is approximately 0.45 eV. However, the attractive region is smaller, and a long-range repulsive barrier is revealed in the present system.

In the H_2O-Li complex calculation,[26−29] several researchers have found a well similar to the wells of the $H_2O + He(2^1S)$ and (2^3S) systems. Therefore, the origin of the well is an attractive interaction of the lone-pair orbitals of the oxygen atom and the half-occupied 2s orbital of He (or Li).

Recently, Tao et al. have calculated the potential surface for the ground-state H_2O-He at the MP4 level with a basis set containing bond functions, and the calculated well depth was

31.8 cm^{-1} (3.94 meV).[30] The very small depth is due to the interaction of one closed shell with another closed shell. In contrast, the interaction of the present system is essentially that of a closed shell and half-filled He 2s shell so that the well is much deeper.

The potential-energy surfaces for the ionized states are much the same as those reported in our previous paper[9] because the basis set used and the scheme for the MCSCF calculation are the same. Isotropic flat surfaces, except for the vicinity of the nuclei, have been obtained for the ionized states.

Figure 2 shows the contour maps of energy widths Γ. The contour lines correspond to logarithms of the widths. The widths show an exponential decrease with increases in the distance between H_2O and He. This exponential decrease has been widely observed for energy widths[4,7,9] and reflects the exponential decay of wave functions. Each width shows a large anisotropy. The partial width for ionization into the B_1 state, $\Gamma(B_1)$, gives a larger value above (and below) the molecular plane on the σ_v plane to which the molecular plane is perpendicular. $\Gamma(A_1)$ takes larger values mainly in the direction of the C_2 axis. The values of $\Gamma(B_2)$ are larger outside the OH bonds than those above and below the molecular plane. These anisotropies of widths are related to those of the electron distribution of the molecular orbitals relevant to the individual ionization.

In the one-electron picture of a Penning ionization, the anisotropies of widths are associated with the target molecular orbitals from which the electrons are ejected when ionization occurs.[31] In the present system, therefore, the anisotropies of $\Gamma(B_1)$, $\Gamma(A_1)$, and $\Gamma(B_2)$ are associated with the $1b_1$, $3a_1$, and $1b_2$ orbitals of the target H_2O molecule, respectively. Because the electron density in the $1b_1$ orbital of H_2O is larger above and below the molecular plane, $\Gamma(B_1)$ has greater values in these areas. It should be noted, however, that $\Gamma(B_1)$ does not vanish on the molecular plane. On the other hand, the $1b_1$ orbital has a node on the molecular plane because the $1b_1$ orbital is a canonical molecular orbital and therefore necessarily belongs to an irreducible representation (b_1 in this case) of the C_{2v} point group. The electron of the $3a_1$ orbital of H_2O distributes more along the C_2 axis so that $\Gamma(A_1)$ is larger along the axis. The values of $\Gamma(B_2)$ are larger outside the OH bonds because the $1b_2$ orbital is extended outside the OH bonds. Similar anisotropies have also been found in $H_2O-He(2^3S)$.[9]

A comparison of the partial widths for a given direction reveals a propensity rule of Penning ionization. For example, $\Gamma(B_1) > \Gamma(A_1) > \Gamma(B_2)$ holds for the approach to the oxygen atom perpendicular to the molecular plane. In this notation, the irreducible representations in the parentheses are for the H_2O^+ system. For this approach, the B_1, A_1, and B_2 states for H_2O^+ correlate to the A′, A′, and A″ states for H_2O-He^+, respectively. Therefore, the widths for totally symmetric A′ states are larger than the width for the nontotally symmetric A″ state for this approach. These results suggest that totally symmetric ionized states for $(M-He)^+$ are favored in a Penning ionization, where M is the target molecule. This is also true for other approaches of He to H_2O. For example, the $\Gamma(A_1)$ is larger than $\Gamma(B_1)$ and $\Gamma(B_2)$ for the approach along the C_2 axis of H_2O. In this case, the A_1, B_1, and B_2 symmetries in the H_2O^+ system again correspond to the A_1, B_1, and B_2 symmetries in the H_2O-He^+ system. Thus, the partial width for the totally symmetric A_1 state is larger than those for the nontotally symmetric B_1 and B_2 states when we consider the H_2O^+ system.

In our previous paper, we analyzed the partial wave expansion of Γ in order to interpret the dominance of ionization into totally symmetric states for a given approach. We reached the conclusion that ionizations associated with orbitals with the pseudo-σ symmetry in regard to the M−He* axis are favored for a given approach of He.[9,32] This conclusion would also be valid for reactions with the singlet metastable He.

The angular distribution of scattered electrons was not calculated in the present paper, but we can deduce the

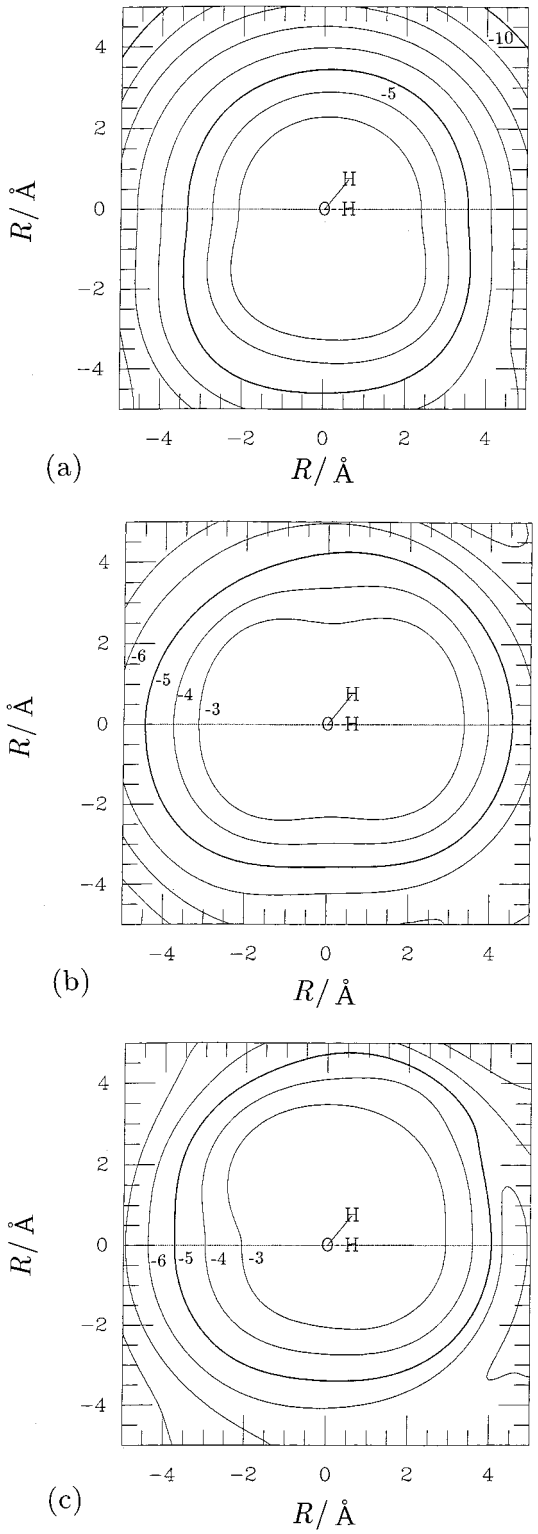

Figure 2. Contour maps of the energy widths Γ for the ionization to three ionized states. The ionized states are (a) $\tilde{X}^2B_1$, (b) $\tilde{A}^2A_1$, and (c) $\tilde{B}^2B_2$. The upper panel is for the molecular plane, and the lower is for the bisector plane that is perpendicular to the molecular plane. Contour lines are for log(Γ/eV). Thick lines are for 10^{-5} and 10^{-10} eV.

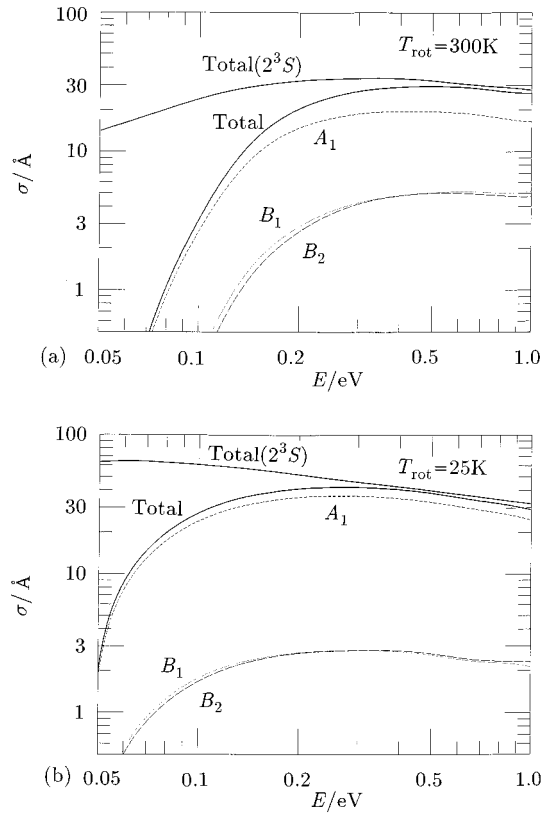

Figure 3. Total and partial Penning ionization cross sections (σ) for $H_2O-He^*(2^1S)$ interaction in the collisional-energy range 0.05−1.0 eV. The H_2O rotational temperature was (a) 300 K and (b) 25 K. The labels "Total" and "Total(2^3S)" indicate total-ionization cross section for the present $H_2O-He^*(2^1S)$ system and that for $H_2O-He^*(2^3S)$, respectively. The labels B_1, A_1, and B_2 indicate partial-ionization cross sections for ionization into the ionized $\tilde{X}^2B_1$, $\tilde{A}^2A_1$, and $\tilde{B}^2B_2$ states, respectively.

distribution from the σ preference and the entrance potential. When the entrance potential is repulsive, the cross section increases with the angle with respect to incident direction owing to the σ preference. When the potential is attractive, however, the memory of incident direction is lost and a flat distribution is obtained over all the angles.[33] Therefore, it is expected in the present system that the cross section increases with angle at lower energies, but a flat distribution is obtained at intermediate and higher energies. The angular distribution of partial ionizations would be similar.

B. Collisiollal-Energy Dependence of the Ionization Cross Sections. Figure 3 shows the energy dependence of the total and partial cross sections. The total cross sections for the triplet state are also shown for comparison. Parts a and b of Figure 3 correspond to the H_2O rotational temperatures of 300 and 25 K, respectively. The calculation was carried out at 150 K, but the result was not significantly different from that at 300 K (not shown). Error bars are not shown in the plots for the sake of clarity. Typical errors are 5−10%.[10]

The lowest rotational temperature of 25 K was selected as a compromise between the temperatures of supersonic jets and the characteristic rotational temperatures (θ_R).[34] Supersonic jets usually achieve a rotational temperature lower than 10 K. The geometric mean of the three characteristic rotational temperatures from the rotational constants of H_2O is 22 K. Because the characteristic rotational temperature is a measure of the spacing between rotational levels, a classical treatment of rotation would be fair for $T = 25$ K.

The partial ionization cross section to produce the A_1 state is the largest of the three in the energy range investigated. There have been no results for partial cross sections of the present system as far as we know. The calculational order of partial cross sections is $\sigma(A_1) > \sigma(B_1) \approx \sigma(B_2)$. For the $H_2O-He^*(2^3S)$ system, relative band intensities in thermal-energy Penning ionization electron spectra show the same order.[6,35,36] This result may be due to a similarity in the anisotropy of the entrance potential and partial widths for both the singlet metastable and the triplet metastable species.

Figure 3a shows that at $T_{rot} = 300$ K, the total ionization cross section decreases in magnitude slightly in the range 0.5−1.0 eV, with a gradient of −0.20 in the log σ versus log E plot, and that the partial cross sections are almost constant in this range. In an experiment, the total ionization cross section has been shown to decrease for collisional energies (E) in the range 0.03−0.2 eV with a gradient of -0.44 ± 0.04,[13] although there have been no absolute cross-section measurements. The present calculation reproduced the decrease of the total ionization cross section at higher energies, although it failed to reproduce this decrease at lower energies.

The total cross sections for the singlet state are found to be smaller than those of the triplet state at lower energies. This is due to the long-range barrier. Because smaller cross sections at lower energies were not reported based on experimental results, the long-range barrier might be an artifact of the present calculation. Even if this is the case, however, it is certain that the repulsive area plays a more significant role for the singlet system than for the triplet system. Further theoretical and experimental investigation may be necessary for this system because this calculation is the first calculation as far as we know, and experimental data are also scarce.

In our previous paper, we discussed the discrepancies between the calculated and experimental values for the triplet system and concluded that the area of the attractive region was underestimated.[10] This was supported by a calculation for a fixed H_2O molecule for which the attractive lone-pair side of the C_2 axis of the H_2O molecule was directed toward the He atom. This underestimation would also be responsible for the discrepancy in the present system in addition to the small long-range barrier.

Ohno et al. have proposed a simple model called the exterior-electron model for the He* Penning ionization and have successfully applied the model to hydrocarbons and their derivatives in order to explain the relative intensities of the Penning ionization spectra.[31,36−38] They classified electrons in the relevant molecular orbitals as being either "exterior" or "interior" electrons and claimed that the population of exterior electrons is proportional to the branching ratio in Penning ionization. However, this model predicts the same branching ratio for the $He(2^1S)$ metastable as for the $He(2^3S)$ metastable. Furthermore, the model predicts that the partial-ionization cross section into the $^2B_1$ state is the largest for a H_2O target molecule.[36] This unsatisfactory prediction is due to the neglect of the difference in spin multiplicities of the metastable species and the neglect of the effect of the entrance-channel PES. The model treats target molecules as being rigid bodies, i.e., as an assembly of van der Waals spheres, and the collision with the metastable species was not considered explicitly.[31,36]

C. Influence of the Effects of Rotational Cooling on the Cross Sections. The plot at $T_{rot} = 150$ K is similar to that at $T_{rot} = 300$ K, but the plot at $T_{rot} = 25$ K (Figure 3b) is significantly different. These results suggest that the cooling effects of rotational temperature are remarkable at very low

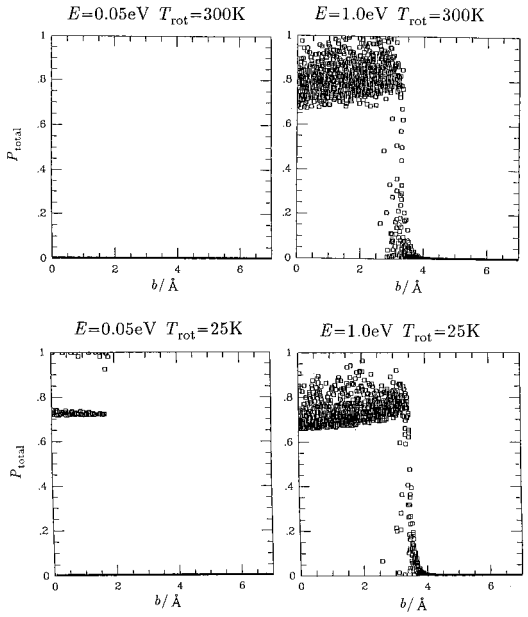

Figure 4. Total-ionization probabilities P_{total} for the impact parameter b. Each square corresponds to each trajectory. E is the collisional energy, and T_{rot} is the rotational temperature of H_2O.

temperatures. The differences between the results at 300 K and those at 25 K are as follows.

(1) The ratio of ionization into the A_1 state to total ionization increases. (2) The total ionization cross section increases over the entire energy range investigated, especially at lower energies. For the triplet case, the total ionization cross section decreases over the collisional energy investigated at $T_{rot} = 25$ K.[10] The appearance of the peak, but not the entire decrease, for the present singlet case is due to the small long-range barrier. (3) The collisional energy at the maximum cross section shifts to the lower-energy side (0.3 eV). This is because of the larger increase in magnitude of cross sections at lower energies.

It is expected from the present calculation that experiments with cooled H_2O beams should exhibit the above three characteristics.

D. Ionization Probability for Each Trajectory. Figure 4 shows the total ionization probability P_{total} for impact parameter b. The results for 2000 trajectories were plotted for each panel. It is noted that almost the same number of trajectories fall into each interval Δb and that the weight of each of the trajectories to the cross sections varies. These characteristics are due to the use of the importance sampling described above.

For $E = 1.0$ eV, the distribution of ionization probabilities does not change very much when the rotational temperature of H_2O is lowered. For slow collision ($E = 0.05$ eV), however, the difference is significant: Although ionization does not occur at $T_{rot} = 300$ K, many trajectories lead to ionization at $T_{rot} = 25$ K. Thus, the effect of rotational cooling is remarkable for slow collisions. Similar results were obtained for the triplet case.[10]

A comparison of the ionization probabilities for the present system with those for the triplet metastable system[10] reveals the following four points. (1) The ionization probabilities are almost zero for $E = 0.05$ eV and $T_{rot} = 300$ K. For the triplet case, the probability is zero or unity. (2) For $E = 0.05$ eV and $T_{rot} = 25$ K, the ratio of trajectories without ionization is higher than for the triplet case. (3) For $E = 0.05$ eV and $T_{rot} = 25$ K, the probabilities are 0, 0.72, or 1.0, and the trajectories with an ionization probability of about 0.72 are more than those with a probability of 1.0. In contrast, for the triplet metastable, the probabilities are zero or unity, and all the trajectories with impact parameters of less than 3 Å give an ionization probability of unity. (4) For $E = 1.0$ eV, although trajectories with impact parameters of less than 3.0 Å ionize with a probability of 0.65−1.0 in the present system, the corresponding trajectories in the triplet system ionize with a probability of almost unity.

The first difference is due to the long-range barrier. The barrier prevents trajectories from going into a small "reactive" area. Here, the term "reactive" means the attractive part of the resonance potential that can retain trajectories in the area for a period long enough for complete ionization to occur. The long-range barrier is responsible for the increase of trajectories without ionization at $E = 0.05$ eV as described in point 2 as well as point 1.

On the other hand, the decrease in trajectories that ionize almost completely (points 3 and 4) is due to the smaller attractive area. For the triplet case, the trajectories that enter the "reactive" region lead to ionization almost completely, and the trajectories that do not go into the "reactive" region lead to little ionization. Thus, in the triplet case, either the ionization probability for trajectories is unity or it vanishes. For the present system, in contrast, the trajectories that go into the reactive, attractive region often go out of the reactive region before complete ionization occurs because the reactive region is not large enough. Therefore, only very few trajectories ionize with a unit ionization probability.

The partial-ionization probability was also investigated. The plots for partial A_1 ionization are fairly similar to those for P_{total}, although fewer points give $P \gtrsim 0.65$, except for $E = 1.0$ eV and $T_{rot} = 300$ K. This is because the A_1 state is the dominant ionization channel: since the partial width for the A_1 state is the largest in the attractive region, the A_1 ionization is dominant. These results are similar to those for the triplet case.

E. Orientation at Minimum Distance and Ionization Probability. Because the resonance potential of the $H_2O-He^*(2^3S)$ interaction has minima in the directions of the lone pairs of H_2O, trajectories are pulled toward this attractive region. The orientation of H_2O with respect to He at the minimum distance is expected to reflect this topological property of the resonance potential.

Figure 5 shows the total-ionization probability (P_{total}) for the angle from the C_2 axis at the minimum distance. We define angle θ_{min} as θ at the $He-H_2O$ minimum distance. θ_{min} is defined to be 0° when the minimum distance point is on the lone-pair side of the oxygen atom and on the C_2 axis.

Trajectories with larger θ_{min} are not found when the rotation of H_2O is slowed for both collisional energies of $E = 0.05$ and 1.0 eV. Trajectories more often assemble in the attractive area at low rotational temperatures because the reduction of the rotational frequency enables He to access the attractive, reactive region. For θ_{min} of less than 15° at $E = 0.5$ eV and $T_{rot} = 25$ K, many trajectories with ionization probabilities of 0.72 or ∼1.0 are revealed. This result is due to the minimum of the potential-energy surface being located at the lone-pair side near the C_2 axis. This is one of the rotational-cooling effects, and a similar result was obtained for the triplet case.

Most of the points have an ionization probability P_{total} of $P_{total} < 0.05$ or $P_{total} > 0.65$ for the $E = 1.0$ eV plots in the present singlet system. The trajectories with a probability of $P_{total} > 0.65$ correspond to "reactive" trajectories that enter the reactive region, and the trajectories with a probability of $P_{total} < 0.05$ correspond to "nonreactive" trajectories that do not enter the reactive region. For the triplet system, the corresponding probability values may be $P_{total} < 0.05$ or $P_{total} > 0.95$. The

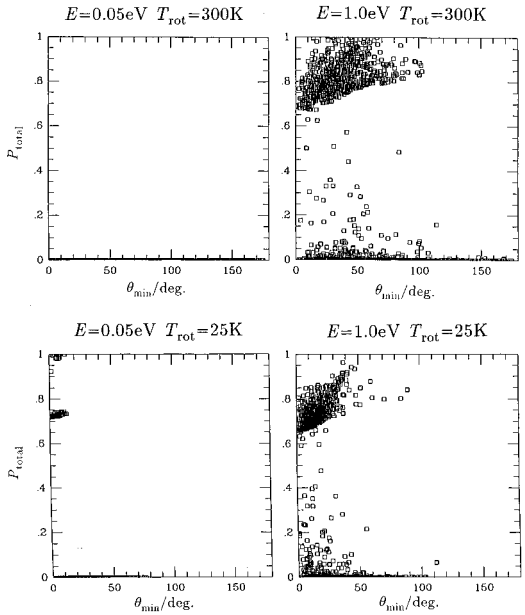

Figure 5. Total-ionization probabilities P_{total} for the angle from the C_2 axis at the minimum distance θ_{min}. The lone-pair side of the H_2O molecule corresponds to the smaller θ_{min}. The origin of the coordinates is the oxygen atom of H_2O. Each square corresponds to each trajectory. E is the collisional energy, and T_{rot} is the rotational temperature of H_2O.

trajectories with medium probability values ($0.05 < P_{total} < 0.65$) are less in the single case than in the triplet case ($0.05 < P_{total} < 0.95$). This may be due to the well in the singlet PES being deeper than the triplet well.

4. Concluding Remarks

We obtained the entrance-channel potential-energy surface and partial-energy width for the $H_2O + He^*(2^1S) \rightarrow H_2O^+ + He + e^-$ system and carried out classical-trajectory calculations on the basis of the PES and the widths obtained. A comparison was made with the triplet metastable counterpart. We have found that a long-range barrier in the present system prevents trajectories from entering the reactive region, and the smaller attractive region causes the trajectories to move out of the reactive region before complete ionization, even though the well depth is greater.

For the present system, experimental study is not enough. The use of metastables with different excited states in experiments, for example, partial-ionization cross-section measurements, combined with theoretical study should enable us to understand the differences in the entrance-channel potential much more.

Acknowledgment. We thank the Computer Center of the Institute for Molecular Science, Okazaki National Research Institute for the use of the SP2 workstation cluster system. The present work has been partly supported by Grants in Aid for Scientific Research on Priority Area "Theory of Chemical Reactions" and for Encouragement of Young Scientists (No. 09740424) from the Ministry of Education, Science, Sports, and Culture of Japan. We are very grateful to the reviewers for their valuable comments.

References and Notes

(1) Nakamura, H. *Int. Rev. Phys. Chem.* **1991**, *10*, 123.
(2) Dunlavy, D. C.; Martin, D. W.; Siska, P. E. *J. Chem. Phys.* **1990**, *93*, 5347.
(3) Dunlavy, D. C.; Siska, P. E. *J. Phys. Chem.* **1996**, *100*, 21.
(4) Siska, P. E. *Rev. Mod. Phys.* **1993**, *65*, 337.
(5) Bentley, J. *J. Chem. Phys.* **1980**, *73*, 1805.
(6) Haug, B.; Morgner, H.; Staemmler, V. *J. Phys. B* **1985**, *18*, 259.
(7) Ishida, T. *Chem. Phys. Lett.* **1992**, *191*, 1.
(8) Ishida, T. *Chem. Phys. Lett.* **1993**, *211*, 1.
(9) Ishida, T. *J. Chem. Phys.* **1995**, *102*, 4169.
(10) Ishida, T. *J. Chem. Phys.* **1996**, *105*, 1392.
(11) Ishida, T.; Horime, K. *J. Chem. Phys.* **1996**, *105*, 5380.
(12) Ishida, T.; Katagiri, H. *Chem. Phys. Lett.* **1997**, *274*, 293.
(13) Allison, W.; Sheldon, J. W.; Muschlitz, E. E., Jr. *J. Electron Spectrosc. Relat. Phenom.* **1981**, *23*, 339.
(14) Feshbach, H. *Ann. Phys.* **1958**, *5*, 357; Feshbach, H. *Ann. Phys.* **1962**, *19*, 287.
(15) Hickman, A. P.; Isaacson, A. D.; Miller, W. H. *J. Chem. Phys.* **1977**, *66*, 1492.
(16) Takahashi, T.; Mori, M. Publ. RIMS. *Kyoto Univ.* **1974**, *9*, 721.
(17) For example, see the following. Press, W. H.; Teukolsky, S. A.; Vetterling, W. T.; Flannery, B. P. *Numerical Recipes in FORTRAN. The Art of Scientific Computing*, 2nd ed.; Cambridge University Press: Cambridge, 1992; Chapter 4.
(18) Dupuis, M.; Watts, J. D.; Villar, H. O.; Hurst, G. J. B. *Quantum Chemistry Program HONDO7*.
(19) Nakamura, H. *J. Phys. Soc. Jpn.* **1969**, *26*, 6.
(20) Miller, W. H. *J. Chem. Phys.* **1970**, *52*, 3563.
(21) Nakamura, H. Private communication.
(22) Marquardt, D. W. J. *Soc. Ind. Appl. Math.* **1963**, *11*, 431.
(23) For example, see the following. Hecht, H. G. *Mathematics in Chemistry. An Introduction to Modern Methods*; Prentice Hall: NJ, 1990.
(24) Hase, W. L.; Feng, D.-F. *J. Chem. Phys.* **1981**, *75*, 738.
(25) Raff, L. M.; Thompson D. L. *Theory of Chemical Reaction Dynamics*; Baer, M., Eds.; CRC Press: Boca Raton, FL, 1985; Vol. III, Chapter 1, p 1.
(26) Trenary, M.; Schaefer, H. F.; Kollman, P. *J. Am. Chem. Soc.* **1977**, *99*, 3885.
(27) Trenary, M.; Schaefer, H. F.; Kollman, P. *J. Chem. Phys.* **1978**, *68*, 4047.
(28) Bentley, J.; Carmichael, I. *J. Phys. Chem.* **1981**, *85*, 3821.
(29) Curtiss, L. A.; Pople, J. A. *J. Chem. Phys.* **1985**, *82*, 4230.
(30) Tao, F.-M.; Li, Z.; Pan, Y.-K. *Chem. Phys. Lett.* **1996**, *255*, 179.
(31) Ohno, K.; Matsumoto, S.; Harada, Y. *J. Chem. Phys.* **1984**, *81*, 4447.
(32) Morgner, H. *Comments At. Mol. Phys.* **1982**, *11*, 271.
(33) Ebding, T.; Niehaus, A. *Z. Phys.* **1974**, *270*, 43.
(34) See, for example, the following. Knox, J. H. *Molecular Thermodynamics: An Introduction to Statistical Mechanics for Chemists*; John Wiley & Sons: Chichester, 1971.
(35) Yee, D. S. C.; Hamnett, A.; Brion, C. E. *J. Electron Spectrosc. Relat. Phenom.* **1976**, *8*, 291.
(36) Ohno, K.; Mutoh, H.; Harada, Y. *J. Am. Chem. Soc.* **1983**, *105*, 4555.
(37) Kajiwara, T.; Masuda, S.; Ohno, K.; Harada, Y. *J. Chem. Soc., Perkin Trans. 2* **1988**, 507.
(38) Ohno, K.; Ishida, T.; Naitoh, Y.; Izumi, Y. *J. Am. Chem. Soc.* **1985**, *107*, 8082.